Effective utilization and characterization of carbon derived from non-biodegradable waste based electrical switches for supercapacitor applications: A green approach

Prabhin VS
T John Institute of Technology
BENITHA V S (vs_benitha@mepcoeng.ac.in)
Mepco Schlenk Engineering College
Jeyasubramanian K
Mepco Schlenk Engineering College
Shantha Selvakumari R
Mepco Schlenk Engineering College
Divya Divakaran
King Mongkut's Institute of Technology North Bangkok: King Mongkut's University of Technology North Bangkok

Research Article

Keywords: Carbon, Char, DESTP, Supercapacitors, e-waste, Electrical switches, Specific capacitance

Posted Date: February 8th, 2023

DOI: https://doi.org/10.21203/rs.3.rs-2516296/v1

Version of Record: A version of this preprint was published at Waste and Biomass Valorization on June 11th, 2023. See the published version at https://doi.org/10.1007/s12649-023-02184-7.

Abstract

This work describes the utilization of carbon (Char) held after the slow pyrolysis of Disposed Electric Switches made of Thermoset Plastic (DESTP) as a high-capacity electrode material for supercapacitor applications. Char is prepared by pyrolysis strategy and exposed to severe milling in high energy planetary ball mill for size reduction. By suspending the pulverised DESTP in silver (Ag) nanoparticles dispersed solution obtained by reducing $AgNO_3$ with hydrazine hydrate as a reducing agent, the DESTP is loaded with Ag nanoparticles. The Energy Dispersive X-Ray Analysis (EDAX) validates the elemental makeup of the manufactured char. The DESTP and Ag@DESTP are coated separately on a low-cost etched brass substrate, and their electrochemical charge-storage properties are investigated using an electrochemical workstation. The specific capacitance of DESTP and Ag@DESTP electrodes are discovered to be 32 $Fg^{-1}$and 67 Fg^{-1}, respectively. The fabricated electrodes provide a maximum volumetric capacitance of 93 $mFcm^{-3}$and 21 $mFcm^{-3}$ with a current density of 5 mA for Ag@DESTP and DESTP electrodes respectively. This work gives a great model of repurposing the e-waste advertising with good electrochemical energy storage applications.

1. Introduction

Innovations and technological advancements have resulted in significant changes in people's lives, economies, and industries [1–5]. Simultaneously, this has resulted in a slew of issues, including the large volume of hazardous garbage and other waste generated by electric products. E-waste is the fastest developing squander stream, expanding at a disturbing rate which causes an irreversible effect on the environment, on the off chance that legitimate strategies are not embraced for the transfer of these wastes [6–9]. The rigorous use of polymer composites has caused environmental issues, since almost all thermosetting plastics are non-biodegradable and possess lot of disposal limits [10, 11]. Despite this, there is a significant increase in energy demand due to technological advancements, which is strongly linked to rising levels of affluence and economic opportunity in much of the world [12–14]. Conversion and storage of energy is clearly a crucial pillar of modern civilization, driven by the reciprocal promotion of economic and environmental development.

Carbon-based supercapacitors are significant large-power devices that continue to dominate the commercial industry, with features including millions of charge/discharge cycles, quick energy pulses, wide range of operating temperatures, and high coulombic efficiency [15–18]. Because of their diverse syntheses, outstanding physicochemical stability and electrical properties, porous carbons have become a common electrode material in carbon based supercapacitors, it can also be generated from conventional biomasses. Several researchers reported the use of carbon obtained from diverse biomasses for supercapacitor applications [19]. Another reason for using such a new carbon normally obtained from woods, barks, leaves, grasses, roots, etc. is owing to its availability and diversity of bio resources. Recent advances in various ways of producing good performance, low-cost activated carbon from respective renewable sources are discussed in the following sections.

Yaglikci*et al* studied the performance of carbon supercapacitors made from waste tea and the electrochemical performances were tested [20]. Fermanelli*et al* studied the carbon extraction from the three types of biomass namely rice husk, peanut shell and wheat straw collected from agro industries, at a pyrolysis temperature of 350–650°C. The study of pyrolysis temperature over the yield of bio-char, liquid (bio-oil) and gaseous (bio-gas) fractions were evaluated for each biomass [21]. Jiangqi Zhou *et al* studied about the biomass derived high capacitance super capacitors wherein they discussed about the electrode materials with various nanostructures to augument exposed active surface areas, widen ionic channels and accelerate electron conductivity [22]. Wenxin Hu *et al* prepared carbonaceous materials from lignocellulosic biomass precursor which has the characteristics of low cost, natural abundance, high specific surface area, and notable electrochemical stability [23].Another study revealed the use of carbon coated core-shell nanomaterials for supercapacitor electrode [24].

In spite of the fact that customizing the geometrical morphologies, pore constructions, and surface capacities in quest for enormous capacitance electrodes is featured in inventive carbon-based material manufacture techniques, fostering another carbon is a new pushed region to store electrical energy in a productive way [25]. From the writing, it is apparent that with the utilization of various kinds of carbon derived from diverse biomasses are utilized for the manufacture of supercapacitor and its qualities were advanced by various scientists [26–30]. Be that as it may, the utilization of carbon got from the pyrolysis of thermosetting plastic widely utilized in the production of electrical appliances like waste electrical switches as supercapacitor electrode materials are not announced up until this point.

Thus, in this specific situation, through this work a novel endeavour is made in regards to the devising of carbon from squander electrical switches (disposed off into the municipal waste) by utilizing slow warm pyrolysis. On heating the waste plastic at 400°C in an oxygen starved atmosphere yields about 60% of carbonaceous content with 2.6% metallic oxides, which on subjected to size reduction by employing high energy ball milling technique. The carbon acquired in 10 nm was additionally stacked with nano silver particles by putting into a suspension having Ag nanoparticles got through the reduction of silver nitrate utilizing hydrazine hydrate as a reducing agent. The dumped carbon (DESTP) and silver stacked DESTP (Ag@DESTP) are utilized as electrode material in supercapacitor application. A supercapacitor electrode with capacitance of 32 Fg^{-1} and 67 Fg^{-1} was attained by depositing DESTP and Ag@DESTP over an etched brass substrate. This study paves the road for acquiring electrode material from waste and toxic polymers that have been discarded into the environment.

2. Materials And Methods

Silver nitrate ($AgNO_3$) and Sodium sulphate (Na_2SO_4) were purchased from Sigma Aldrich and was used without any modification for depositing Ag over DESTP on brass substrate. Brass substrate with1 mm thickness was purchased from the local Indian market and it was sized in the dimensions of 1 cm × 3 cm as current collector. Before depositing Ag on the char, the substrate was cleaned by abrading with an abrasive paper. The dirt particles were removed by washing with distilled water followed by sonicating in acetone.

2.1 Scrap material

Commercially available thermosetting electrical switches were collected from the municipal waste and the metallic parts were removed manually. The non-metallic thermoset plastic was then cleaned with distilled water to remove the dirt and manually crushed into small pieces.

2.2 Preparation of DESTP

About 5 g of waste switches were weighed and crushed into a fine powder mechanically. Then the powdered sample was taken in a silica crucible, covered with a lid. This process not allows the intimate mixing of air with the plastic powder. The contents were then heated at 400° C in a muffle furnace for a period of 3 hrs. During heating, the organic contents present in the switches were decomposed in the form of H_2O (g), CO (g), etc., leaving2.44 g of carbon powder as a residue (approximately 50%). After the pyrolysis, the carbon content retained on the crucible was grounded to a fine powder using pestle and mortor. The same process was repeated to get bulk quantity of carbon powder from more amounts of switches. About 20 g of powdered carbon was taken in a high energy ball mill (Fritsch, Germany) with a powder to ball ratio of 1:10. The tungsten carbide balls were used to ground the carbon powder into nano size and the milling process was carried outat a speed of 300 rpm. After 2 hrs of grinding, the obtained carbon powder in nano size was collected and stored in vacuum.

2.3 Loading of nano Ag over carbon powder

About 0.01 M $AgNO_3$ (1.70 g) was dissolved in 50 ml distilled water. Equimolar ratio of hydrazine hydrate taken in 30 ml of distilled water was slowly added with constant stirring to the $AgNO_3$ solution. After 3 hrs of stirring, a yellow-colored solution was obtained confirms the formation of nano size silver particles. Also, it was confirmed by recording UV spectra in which it exhibits a λ_{max}at 420 nm confirms the formation of Ag nanoparticles[31]. After transferring the yellow color solution into a 250 ml beaker, 1 g of nanosize carbon powder was slowly introduced with constant stirring. Addition of carbon powder was continued for about 60 minutes. After 1 hr, settling of Ag@DESTP was noticed leaving a clear supernatant liquid. This fact supportsthat the nano Ag particle were found adsorbed over the carbon powder. Nanosize C and Ag loaded on C were also confirmed from FESEM with EDAX and XRD studies.

2.4 Fabrication of electrode

Low-cost brass substrate having composition of 66% Cu and 34% Zinc was used a current collector. The porosity on the brass substrate was developed by soaking in 70% HNO_3 for 5 seconds. During the soaking process, the copper present in the brass substrate reacts with the acid and gets detachedout leaving pores on the substrate. The brass substratewas then washedthoroughly with distilled water to remove the traces of nitric acid adhered on thesurface. The cleaned substrate was preheated at a temperature of 40°C in a hot plate. 0.01 g of DESTP and Ag@DESTP was individually dispersedin acetone, wherein the uniform distribution of carbon powder and Ag@DESTP were obtained by sonication. Then the respective suspensions weredeposited on the preheated substrate by drop casting method. About 1 ml of the suspension containing carbon powder and Ag@DESTP were placed on the substrate

kept over the hot plate maintained at 50–60°C. Complete dropping of 1 ml of the suspension produces the carbon coated and Ag@DESTP coated electrodes.

3. Results And Discussion

3.1 XRD analysis

X-ray powder diffraction (XRD) is used for the analysis of phase purity and crystallinity of materials. XRD patterns were captured from a Rigaku Ultima IV automatic multipurpose X-Ray Diffractometer (USA) with Cu Kα radiation (λ = 1.5418 Å) operating at 40 kV with 30 mA current. Data were acquired in the range of 20° – 80° and the XRD peakscharacteristics to the prepared DESTP [Fig. 1(a)], consists of various peaks, not all are originated from carbon. The diffraction peak obtained at 2θ = 27.15° (002) corresponds to the carbon[JCPDS No. 08-0415]formed from the plastic waste[32]. In view of the fact that, during the manufacture of electrical switches from bakelite, various additives were added to obtain the required characteristics. The peak corresponding to 27.83° (110) and 63.96° (204) originated from TiO_2[JCPDS No. 71-1169][33], the peaks appeared at 2θ = 31.45°(100), 46.96°(102), 69.55°(201) were obtained from ZnO[JCPDS No. 36-1451][34], the peak at 2θ = 39.34° (102) from SiO_2[JCPDS No. 85–0335][35], the peaks at 2θ = 55.12°(211) from BaO[JCPDS No. 89-8425][36]and a peak noticed at 2θ = 77.61°(311)from Ag[JCPDS No. 04-0783][37]. The peaks originated from TiO_2,ZnO,SiO_2,BaO and Ag were due to the presence of additives added while manufacturing and converted into their respective oxides during pyrolysis. It is observed that, different oxides present in the DESTP were well matched with the compounds present in EDAX analysis. It is observed that, due to the pyrolysis process, the depth of the amorphous carbon peak becomes more exposed and moves to 26°-27°which is closely associated with the processes of graphitization of the organic component and the development of the nanocrystalline structure of the matrix[38, 39].

Figure 1(b) shows the XRD pattern of silver nanoparticles, in which the peaks appeared at 2θ = 38.26°, 44.44°, 64.61°, 77.55° are matched well with the Miller indices of (111), (200), (220), (311) reflections of the face-centered cubic structure of metallic silver with the standard JCPDS card No. 04 0783 [37, 40]. Figure 1(c) is the XRD pattern of Ag@DESTP, in which all the peaks indexed in Fig. 1(a)is appeared along with the silver peaks. This fact supports that the nano Ag particle were found loaded (adsorbed) over the carbon powder and a decrease in the intensities is attributable to the Ag doping.

3.2 FESEM analysis

Field Emission Electron Microscope is used to examine the surface morphology and microstructure of the obtained carbon and Ag loaded carbon. FESEM images are captured through FESEM-Carl Zeiss MA 15/EVO 18 electron microscope (Germany). The FESEM image of the brass and etched brass substrate found after dipping in nitric acid is shown in Fig. 2(a) & (b). From Fig. 2(b), it is clear that the porous nature of the brass substrate is because of the removal of Cu atoms from the brass substrate. The reaction involved in the removal of Cu atoms is given in the Eq. 1.

$$3\,Cu + 8\,HNO_3 = 3\,Cu(NO_3)_2 + 2\,NO^{\uparrow} + 4\,H_2O \quad (1)$$

The porous structures are formed as a result of gas generation. Suchlike porous nature of the current collector is more important in collecting and storing the charges. Figure 2 (c) depicts the porous structure of DESTP with an average pore size of around 200 nm. The image also shows the dissection with trifling and profound traps, which are significant for charge transportation and energy storage property [41, 42]. This geometry enhances the electrode surface area, leading to a rise in junction area between the electrode material and the electrolyte. Figure 2 (d) shows the FESEM image of Ag@DESTP with a mesoporous nature, and the particles are agglomerated and the individual particle is found to be in 10 nm size.

Figure 3(a-d) is the EDAX analysis of brass substrate, etched brass, DESTP and Ag@DESTP respectively. The EDAX clearly reveals the presence of Cu and Zn in Fig. 3(a) & (b) and the EDAX graph of DESTP and Ag@DESTP (Fig. 3(c) & (d)) reveals the presence of C with other elements like Ti, Zn, Ba, Si, Ag as confirmed from XRD. Various elements present in the brass substrate, etched brass substrate, DESTP & Ag@DESTP with the atomic weight percentages are displayed in Fig. 4(a) & (b), from this it is observed that around 4.27% of copper atoms have been etched from the substrate after immersion in 70% HNO_3 for few seconds. The expulsion of copper atoms from the brass substrate paves a way for the better adherence of DESTP and Ag@DESTP. Besides the conventional elements like Cu and Zn from the substrate, after coating C, it exhibits a characteristic peak for carbon and nitrogen. In addition to these, the EDAX clearly revealed the presence of atoms like Ti, Zn, Ba, Si which were all originated from the additives. Interestingly, the Ag@DESTP additionally exhibits a characteristic peak for Ag, obviously obtained from the loading of silver nanoparticles.

3.3 BET analysis

The porosity nature of the DESTP and Ag@DESTP materials is investigated using N_2 absorption/desorption isotherms [Fig. 5(a) & (b)]. The behavior of N_2 absorption/desorption resembles that of a type IV isotherm including hysteresis. At low pressure, the adsorption and desorption isotherms are superimposed, owing to the adsorption of gases in the micropores. As the pressure is increased, due to the capillary agglomeration phenomenon, the isotherms increase rapidly forming a lag loop. The surface area (SA) is vital for improving the performance and energy storage capability of the electrodes. Employing BET analysis, the SA for DESTP and Ag@DESTP is found to be 238.98 m^2 /g and 310.71 m^2/g, respectively.

The pore size matrix of DESTP and Ag@DESTP are shown in Fig. 5c & d, which were calculated using the BJH model. It is observed from the curve that the size of the pores are around 40 nm in DESTP [Fig. 5c] and 6 nm in Ag@DESTP [Fig. 5d], attributing the presence of micropores.

3.4 Electrochemical analysis

3.4.1 CV Analysis

Electrochemical investigations are carried out to measure the characteristics of the fabricated supercapacitor electrodes. Each electrochemical study was performed via the electrochemical workstation (CHI660C, USA). A standard three-electrode arrangement was used in this study consists of a standard calomel cathode (SCE) as a reference electrode, platinum wire as a counter electrode and the fabricated electrode as a working electrode respectively. All experiments were performed at room temperature with 1 M aqueous sodium sulphate solution as the electrolyte. Figure 6 (a) & (b) shows the CV curves of the DESTP and Ag@DESTP electrodes performed in a potential window of -0.8 V– 0V at different scan speeds of 5,10, 25,50,75 and 100 mVs^{-1} respectively. The CV curves show the significant increase of specific capacitance after deposition of silver nanoparticles. From the voltametric profile, an increase in the electric double layer capacitance is observed for Ag@DESTP electrode. The specific capacitances of DESTP and Ag@DESTP electrodes were determined using the following equation [43–45].

$$C_{sp}=\frac{1}{mV(v2-v1)}\int_{v2}^{v1} I\,(v)\,dv \quad (2)$$

where, dv is the difference in potential, m is the mass of the electrode active material deposited, I(V) is the current density, v is the scan rate in seconds and v_1 and v_2 are the cathodic and the anodic potential.

The mass of the active materials deposited over the etched brass current collectors were determined by weighing the substrate before and after deposition of active materials employing digital balance. The mass of the electrode active materials deposited over the electrode was 0.2mg and 0.23 mg in the case of DESTP and Ag@DESTP electrodes respectively. The specific capacitance associated with DESTP and Ag@DESTP electrodes are 32 Fg^{-1} and 67 Fg^{-1} with the scan rate of 5 mVs^{-1} respectively. As the scan rates are increased, the specific capacitance ofDESTP electrodes is decreased to 22, 16, 10, 8 and 5 Fg^{-1} at the scan rates of and 10,25,50,75 and 100 mVs^{-1} respectively. Eventually, the specific capacitance of Ag@DESTP electrode is decreased to 36, 25, 16, 12 and 10 Fg^{-1} at the scan rates of 10,25,50,75 and 100 mVs^{-1} respectively. This outcome suggests a critical job that silver nanoparticles loaded on the Ag@DESTP cathode significantly expanding the exposed surface area accessible for the greater occurrence of the electric double layer process in an effective manner. A non-symmetric profile with regards to the charging/releasing of the electric double layer is likewise observed. As indicated by the cyclic voltammograms, the best behaviour of an electric double layer capacitance is appeared in the form of a symmetric rectangular shape [46–48]. The deficiency of DESTP and Ag-DESTP electrodes symmetricity might be related to conceivable reversible pseudo-faradaic responses that happened in a likely area at around-0.6V and − 0.2 V. Furthermore, as electric double layer discharging happens, the resulting current profile gets more inclined due to the fact that the ions leave the Ag pores with strain most likely due to capillary effect [49–52]. Comparison of specific capacitance values of various carbonaceous materials along with their data available is given in Table 1.

Table 1
Comparison of specific capacitance

Sl.No.	Material	Specific capacitance	Reference
1	Graphene and carbon nanofiber (CNF)	51 Fg^{-1} at 1 Ag^{-1}(CNF)	[53]
		409 Fg^{-1} at 1 Ag^{-1}(MnO/CNF)	
2	Carbon derived from areca fibres	34 Fg^{-1} at 5 mVs^{-1} (Non activated carbon)	[54]
		64 5 mVs^{-1} (activate carbon)	
3	Hybrid fibers assembled from $MoSe_2$/grapheme heterostructures	20.7 Fg^{-1} at a current density of 0.1 A cm^{-3}(bare graphene fibers)	[55]
		135.1 Fg^{-1} at a current density of 0.1 Acm^{-3} ($MoSe_2$/graphene hybrid fibers)	
4	Carbonized PMF resin	58 Fg^{-1} at 2 mVs^{-1} (C700)	[56]
5	Carbon derived from waste compact disk which is activated by a single step process of carbonization followed by activation	51 Fg^{-1} at 10 mVs^{-1}	[57]

Figure 7(a) & (b) show the galvanostatic charge discharge (GCD) curves of DESTP and Ag@DESTP electrodes respectively. The pattern of the curve is not symmetrical in nature and the discharge time of Ag-DESTP electrode is comparatively high, which proves its good charging capacity attributable to the greater stacking of silver on the open-pores of the carbon. Moreover, the contribution of Ag nanoparticles results in the large increase of electric double layer capacitance than pseudo capacitance which could be noticed from the equivalent circuits of Ag@DESTP and DESTP. The double layer capacitance (Q_{dl}) of DESTP and Ag@DESTP obtained from equivalent circuit are 55 µF and 355 µF whereas, an increase of diffusion capacitance Q_d is not observed after incorporating Ag nanoparticles.

The hysteresis noticed in the charge discharge curve is due to IR drop in electrolyte resistance, change in internal resistances and electrode materials [58–61]. The estimates of the IR drop from the DESTP and Ag@DESTP electrodes were 0.25 V and 0.36 V respectively. A considerable increase in the IR drop of Ag@DESTP electrode is attributed to the large surface area and volume change that occurs during Ag doping process. Also, as the void spaces in the DESTP are filled by Ag nanoparticles, results in the decrement in the contact spots of the etched current collector with the Ag@DESTP composite materials owing to increase in IR drop of the electrode. Furthermore, the electrochemical characteristics were

evaluated employing GCD curve recorded by the increasing current densities. It is obvious from the Fig. 7 (c) that the curve follows a diminishing specific capacitance trend as the scan rate increases. This is explained by Randles-Sevcik equation in which, the current involved in the redox reaction is the square root of the scan rate and linearly related to the concentration of the electro active substance. The Randle-Sevcik equation is given below [62–64].

$I_p=kn^{3/2}AD^{1/2}Hf^{1/2}$ **(3)**

where, n represents the number of electrons, H is the solution concentration in moles/L, f is the scan rate per time and D is the diffusion co-efficient in cm^2. At lower scan rates, the dissemination of particles into the interlayer of the electrodes happens subsequently, instigating a greater number of active sites for charge-transfer responses [65, 66].

Figure 7(d) depicts the reduction of volumetric capacitance in analogous to the current density starting from 5 mA to 7 mA in Na_2SO_4 electrolyte solution. The decrease in specific capacitance with the augument in current density is because of the fact that, at higher current densities, the time taken for the charging process is very less which leads to less ionic penetration at the surface of the electrode as matched with low current density. The formula used to determine specific capacitance from GCD curve is given in equation [67, 68].

$$\mathrm{C}v = \frac{i\Delta \mathrm{t}}{v\Delta \mathrm{V}}$$

4

where, *i* is the charge current, Δt represents the discharge time, *v*is the effective volume of the electrode and ΔV, the potential window (0V -0.8V). The electrodes provide the maximum volumetric capacitance of 93 $mFcm^{-3}$and 21 $mFcm^{-3}$ toward a current density of 5 mA for Ag@DESTP and DESTP electrodes respectively. Figure 7(e) & (f) shows the specific capacitance retention of DESTP and Ag@DESTP electrodes recorded at the sweep rate of 100 mVs^{-1} for 5000 cycles. The electrodes retain the specific capacitance of 93% and 91% of its initial values for DESTP and Ag@DESTP electrodes respectively.

The other vital parameters that affect the performance of supercapacitors are energy density and power density. The E_d values of the supercapacitor electrodes could be analysed from the CV curves using the following formula [69, 70]

$$Ed = \frac{CspV^{2}}{2}$$

5

Where *V* is the potential window and C_{sp} is the specific capacitance obtained from CV with scan rate of 5 mVs^{-1}. The power density is obtained by dividing the energy density by time taken toward the completion of one periodic cycle using the expression [71].

$$Pd = \frac{Ed}{t}$$

6

The energy and power density calculated from above expression for DESTP and Ag@DESTP electrodes are 10.24 Wh/kg & 24.576 KW/Kg and 21.44 Wh/kg & 9.89 KW/kg respectively. Extraordinary power and energy density in both the electrodes are attributed to the low inner resistance to charging and discharging of electrodes which is replicated in EIS studies (Electrochemical impedance spectroscopy) as well.

3.4.2 EIS Studies

Electrochemical impedance spectroscopy is a method used to determine the kinetic properties of the active component's as well as the electrodes capacitive nature. The resulting impedance is shown as real and imaginary components of a supercapacitor as frequency dependent capacitance values [72, 73]. EIS analysis was carried out over a DC voltage with a sinusoidal signal of small amplitude of 10 mV spanning between the frequency of 0.1 Hz to 100 kHz.

Figure 8 (a) & (c) depicts the comparison between the Nyquist plot of DESTP and Ag@DESTP electrodes. Figure 8(b) & (d) are the zoomed curves of Fig. 8(a) & (c), displaying the high frequency intersection of Nyquist plot. The enlarged Nyquist plot attributes a quasi-semicircle type behaviour that is a non-vertical line of intermediate frequency obtained by ion transport, restrictions in volumetric electrolyte transport, ion transport routes from the volumetric electrolyte to the porous electrode surface caused by electrode roughness and non-uniformity of the electrode pore size [74]. The intersection between the horizontal axis and the vertical axis is aligned to the y axis at lower frequencies and is related to the frequency dependent internal resistance and the equivalent resistance of the electrode [75–77]. The Equivalent Series Resistance (ESR) of DESTP and Ag@DESTP electrodes are extracted from the intersection of the real axis in the high frequency region of the Nyquist plot and are 28 Ω and 5 Ω, accordingly.

Furthermore, the Nyquist graph of the electrodes has two curve sections, one with 45° slopes that intersects at higher frequency and a lower frequency region that depicts the component's capacitive behaviour. The capacity of the ions to infiltrate the pores at higher frequencies is largely limited, owing to the electrodes repulsive behaviour. The curve shows a strong ramp of imaginary capacitance aligned to the y-axis at the middle frequency, indicating good capacitance behaviour of the electrodes. The knee frequency, which is associated with the initial frequency where electrolyte diffusion begins, is found at the intersection of the intermediate and high frequency regions.The electrode extravagantly works as a capacitor above the knee frequency, and its contribution to the specific capacitance is bigger in this time scale.The knee frequency of DESTP and Ag@DESTP electrodes is 2 Hz and 9Hz, respectively, as shown in Fig. 8 (b) & (d). For the DESTP and Ag@DESTP electrodes, the equivalent circuit gives values of 4.80 Ω & 1 Ω and 8.82 Ω &5.24 Ω for solution resistance R_s and R_{ct}, which is the charge transfer resistance.

Figure 8 (e) & (f) is the equivalent circuit design obtained for DESTP and Ag@DESTP electrodes, in which the solution resistance R_s is connected to the other component since the current flows to the electrolyte at different frequencies. The charge transfer resistance of Ag@DESTP was low owing to its higher capacitance. The double layer charge is represented by the constant phase component Q_{dl}. When the frequency is reduced in the high frequency zone, the impedance provided by Q_{dl} increases quickly, allowing the current to pass through the charge transfer resistance R_{ct}. The ion-desorption resistance of DESTP and Ag-DESTP electrode materials is determined to be 21.05 Ω and 30.38 Ω, respectively.A suitable electrode material must always have a high ion desorption resistance value. The current flows through R_{des} (desorption resistance) at low frequencies because the diffusion capacitance Q_d has a very high impedance. The diffusion capacitance value of the Ag@DESTP electrode is much larger than that of the DESTP electrode, implying that the hybrid Ag@DESTP electrode has a higher specific capacitance value.

The phase angle versus log frequency diagram, often known as the bode plot, depicts the impedance characteristics of supercapacitors. Electrochemical nature of a supercapacitor varies between that of a pure resistor with phase angle 0°and that of a pure capacitor with a phase angle of 90°. At higher frequencies, the supercapacitor electrode behaves like a pure resistor since capacitance is inversely proportional to frequency, resulting in a near zero impedance for a capacitor [78]. Figure 8 (g) shows the phase angle vs frequency plot of DESTP and Ag@DESTP electrodes, with a maximum phase angles of 28° and 49°. The increase in the phase angle of Ag@DESTP is due to the enhanced faradaic contribution of the electrode by silver particles. The time constant determined from maximum phase angle for DESTP and Ag@DESTP are 1 s and 0.301 s respectively. Low time constant produced by Ag@DESTP electrode have small time response which reveals the better performance of the supercapacitor electrode.

The capacitive characteristics of the electrodes are further investigated by utilising Equations (7 & 8) to get the complex capacitances with respect to the given frequency [78].

$$C'_{\omega} = \frac{-Z''}{\omega \times |Z''\omega|^2} \quad (7)$$

$$C''_{\omega} = \frac{-Z'}{\omega \times |Z\prime\omega|^2} \quad (8)$$

where, C'_{ω} and C''_{ω} are the real and imaginary capacitances and ω is the angular frequency. Figure 9(a) & (b) depicts the real capacitance of the DESTP and Ag@DESTP electrodes respectively. In both the electrodes, the real portion capacitance was initially large at lower frequencies and then gradually decreased as the frequency increased. This could be influenced by the penetration of electrolytes into the deep pores of the nanostructures at lower frequencies, while at higher frequencies electrolyte ions could only reach the top surface materials. Figure 9(c) & (d) shows the imaginary capacitance of DESTP and Ag@DESTP electrodes. The reciprocal of f_o gives the dielectric relaxation time constant τ_o, and f is the frequency at which the imaginary part capacitance reaches its highest value. The dielectric relaxation time constants for DESTP and Ag@DESTP electrodes are 0.7 s and 0.1s, respectively, giving a similar

time constant calculated from bode plot. Within this dielectric relaxation time constant f_o, 50% of the capacitance for the entire electrode system is achieved.

4. Conclusion

Based on the current study, the carbon obtained from the e-waste (thermoset plastic) was significantly used as an energy storage material. Size reduction of the obtained char was done employing high energy ball milling technique. The charge storing capacity of the carbon was further enhanced by loading silver nano particles generated via wet chemical method. A simple drop casting method was adopted to coat the DESTP and Ag@DESTP material on the low cost brass substrate. The findings reveal the prepared electrode with etched brass substrate has a specific capacitance of 32 Fg^{-1}, yet on addition of Ag significantly increasesthe specific capacitance to a value of 67 Fg^{-1}. Cyclic stability of the electrodes was evaluated by running the cyclic voltammogram which displayed the retention of 93% and 91% for DESTP and Ag@DESTP electrodes at the scan rateof100 mVs^{-1} for 5000 cycles. Moreover, the results obtained from the Nyquist and Bode plots of low solution resistance and time constant provide insight into the reason for exceptional power density. This study focuses to achieve the recycling of carbon obtained from e-waste (thermoset plastic) to be used as electrode material in supercapacitor. The Ag@DESTP gave better performance after incorporating Ag nanoparticles and the results are advocated by different characterization techniques like FESEM, BET, and CV. Following a comparison of these samples with the literature, it is obvious that Ag@DESTP electrode performed respectfully in the area of carbon-based composites. This in fact, encourages the fabrication of supercapacitor electrode using DESTP-activated carbon.

Declarations

Acknowledgement:

The authors would like to thank the Principal and the Management of MEPCO Schlenk Engineering College, Sivakasi for providing necessary experimental facilities to carry out this research work.

Ethical Approval

Not Applicable

Competing interests

The author(s) declared no competing interest with respect to the research, authorship, and/or publication of this article

Authors' contributions

V.S.Prabhin - Conceptualization, Investigation, Methodology, Writing Original Draft, Visualization and Data Curation.

V.S.Benitha - Resources, Formal analysis, Validation, Writing - Review & Editing, Project Administration, Supervision

K.Jeyasubramanian & R.Shantha Selvakumari - Visualization and Supported for data interpretation.

Divya Divakaran - Conceptualization, Writing - Review & Editing, Visualization and Supported for data interpretation.

Funding

No funding is received for this research work.

Availability of data and materials

The data that support the findings of this study are available on request from the corresponding author. The data are not publicly available due to privacy or ethical restrictions.

References

1. Sima, V., Gheorghe, I.G., Subić, J., Nancu, D.: Influences of the Industry 4.0 Revolution on the Human Capital Development and Consumer Behavior: A Systematic Review. Sustainability. 12, 4035 (2020). https://doi.org/10.3390/su12104035
2. Soam, A., Kumar, R., Thatoi, D., Singh, M.: Electrochemical Performance and Working Voltage Optimization of Nickel Ferrite/Graphene Composite based Supercapacitor. J Inorg Organomet Polym Mater. 30, 3325–3331 (2020). https://doi.org/10.1007/s10904-020-01540-7
3. Shrestha, L.K., Shrestha, R.G., Joshi, S., Rajbhandari, R., Shrestha, N., Adhikari, M.P., Pradhananga, R.R., Ariga, K.: Nanoarchitectonics of Nanoporous Carbon Materials from Natural Resource for Supercapacitor Application. J Inorg Organomet Polym Mater. 27, 48–56 (2017). https://doi.org/10.1007/s10904-017-0548-2
4. Zhang, K., Shang, Z., Wu, S., Wang, J., Sheng, W., Shen, X., Zhu, M.: Commercialized Benzoxazine Resin-Derived Porous Carbon as high Performance Electrode Materials for Supercapacitor. J Inorg Organomet Polym Mater. 27, 1423–1429 (2017). https://doi.org/10.1007/s10904-017-0596-7
5. Britto, J.F., Samson, V.A.F., Bernadsha, S.B., Madhavan, J., Raj, M.V.A.: Synthesis of rNiCo Nanocomposite - As an Electrode Material for Supercapacitor Applications. J Inorg Organomet Polym Mater. 32, 4601–4613 (2022). https://doi.org/10.1007/s10904-022-02455-1
6. Britto, J.F., Samson, V.A.F., Bernadsha, S.B., Madhavan, J., Raj, M.V.A.: Synthesis of rNiCo Nanocomposite - As an Electrode Material for Supercapacitor Applications. J Inorg Organomet Polym Mater. 32, 4601–4613 (2022). https://doi.org/10.1007/s10904-022-02455-1

7. Hariganesh, S., Vadivel, S., Paul, B., Kumaravel, M., Rajendran, S., Balasubramanian, N., Dhar, S.S.: Magnetically Recoverable Graphene Oxide Wrapped CuCo2S4/Iron Oxides Composites for Supercapacitor Application and Fenton Degradation of Organic Molecules. J Inorg Organomet Polym Mater. 31, 1978–1991 (2021). https://doi.org/10.1007/s10904-020-01840-y
8. Lambert, S., Wagner, M.: Environmental performance of bio-based and biodegradable plastics: the road ahead. Chem. Soc. Rev. 46, 6855–6871 (2017). https://doi.org/10.1039/c7cs00149e
9. Yung Li Loh, N., Ying Pang, H., Ting Tee, W., Yan Zhang Hiew, B., Hanson, S., Chong, S., Thangalazhy-Gopakumar, S., Gan, S., Yee Lee, L., Yee Lee Lai-YeeLee, L.: Synthesis of Renewable and Cost-Effective Bioplastic from Apple Waste: Physicochemical and Biodegradability Studies. Waste and Biomass Valorization 2022. 1, 1–18 (2022). https://doi.org/10.1007/S12649-022-01983-8
10. Sánchez-Safont, E.L., Aldureid, A., Lagarón, J.M., Gamez-Perez, J., Cabedo, L.: Effect of the Purification Treatment on the Valorization of Natural Cellulosic Residues as Fillers in PHB-Based Composites for Short Shelf Life Applications. Waste Biomass Valorization. 12, 2541–2556 (2021). https://doi.org/10.1007/S12649-020-01192-1/TABLES/2
11. Tran, D.T., Joubert, A., Venditti, D., Durecu, S., Meunier, T., le Bihan, O., Fiani, E., le Coq, L.: Characterization of Polymer Waste Containing Nano-fillers Prior its End-of-Life Treatment. Waste Biomass Valorization. 8, 2463–2471 (2017). https://doi.org/10.1007/S12649-016-9757-0/FIGURES/5
12. Sajjad, M.: Recent Advances in SiO2 Based Composite Electrodes for Supercapacitor Applications. J Inorg Organomet Polym Mater. 31, 3221–3239 (2021). https://doi.org/10.1007/s10904-021-01899-1
13. Spathi, C., Vandeperre, L.J., Cheeseman, C.R.: Production of Lightweight Fillers from Waste Glass and Paper Sludge Ash. Waste Biomass Valorization. 6, 875–881 (2015). https://doi.org/10.1007/S12649-015-9370-7/TABLES/2
14. Ibáñez-García, A., Martínez-García, A., Ferrándiz-Bou, S.: Influence of Almond Shell Content and Particle Size on Mechanical Properties of Starch-Based Biocomposites. Waste Biomass Valorization. 12, 5823–5836 (2021). https://doi.org/10.1007/S12649-020-01330-9/FIGURES/13
15. Miao, L., Song, Z., Zhu, D., Li, L., Gan, L., Liu, M.: Recent advances in carbon-based supercapacitors. Mater Adv. 1, 945–966 (2020). https://doi.org/10.1039/D0MA00384K
16. Wongwuttanasatian, T., Chaochaiyaphum, W., Seithtanabutara, V.: Valorization of MSW Incinerator Fly Ash for Epoxy-Based Composite for Interior Light Partition Application. Waste Biomass Valorization. 13, 2795–2814 (2022). https://doi.org/10.1007/S12649-022-01684-2/FIGURES/16
17. Lendvai, L., Singh, T., Fekete, G., Patnaik, A., Dogossy, G.: Utilization of Waste Marble Dust in Poly(Lactic Acid)-Based Biocomposites: Mechanical, Thermal and Wear Properties. J Polym Environ. 29, 2952–2963 (2021). https://doi.org/10.1007/S10924-021-02091-9
18. Bakshi, P., Pappu, A., Bharti, D.K., Patidar, R., Gupta, M.K.: Sustainable Development of Particulate Reinforced Composites by Recycling Marble Waste for Advanced Construction Applications: Ultra-low Water Absorption, Remarkable Thermal and Mechanical Behaviour. Waste Biomass Valorization. 12, 6449–6464 (2021). https://doi.org/10.1007/S12649-021-01473-3/FIGURES/10

19. Spada, J.C., Jasper, A., Tessaro, I.C.: Biodegradable Cassava Starch Based Foams Using Rice Husk Waste as Macro Filler. Waste Biomass Valorization. 11, 4315–4325 (2020). https://doi.org/10.1007/S12649-019-00776-W/TABLES/6
20. Yaglikci, S., Gokce, Y., Yagmur, E., Aktas, Z.: The performance of sulphur doped activated carbon supercapacitors prepared from waste tea. Environ Technol. 41, 36–48 (2020). https://doi.org/10.1080/09593330.2019.1575480
21. Fermanelli, C.S., Córdoba, A., Pierella, L.B., Saux, C.: Pyrolysis and copyrolysis of three lignocellulosic biomass residues from the agro-food industry: A comparative study. Waste Management. 102, 362–370 (2020). https://doi.org/10.1016/j.wasman.2019.10.057
22. Zhou, J., Zhang, S., Zhou, Y.-N., Tang, W., Yang, J., Peng, C., Guo, Z.: Biomass-Derived Carbon Materials for High-Performance Supercapacitors: Current Status and Perspective. Electrochemical Energy Reviews. 4, 219–248 (2021). https://doi.org/10.1007/s41918-020-00090-3
23. Hu, W., Xiang, R., Lin, J., Cheng, Y., Lu, C.: Lignocellulosic Biomass-Derived Carbon Electrodes for Flexible Supercapacitors: An Overview. Materials. 14, 4571 (2021). https://doi.org/10.3390/ma14164571
24. Xu, J., Wang, X., Zhou, X., Yuan, N., Ge, S., Ding, J.: Activated carbon coated CNT core-shell nanocomposite for supercapacitor electrode with excellent rate performance at low temperature. Electrochim Acta. 301, 478–486 (2019). https://doi.org/10.1016/j.electacta.2019.02.021
25. Ariyanto, T., Zhang, G.R., Kern, A., Etzold, B.J.M.: Preparation of hollow mesoporous carbon spheres and their performances for electrochemical applications. IOP Conf Ser Mater Sci Eng. 316, 012018 (2018). https://doi.org/10.1088/1757-899X/316/1/012018
26. Hou, Z., Luo, M., Yang, Y., Zhou, J., Liu, L., Cai, J.: Algae-based carbons: Design, preparation and recent advances in their use in energy storage, catalysis and adsorption. New Carbon Materials. 36, 278–303 (2021). https://doi.org/10.1016/S1872-5805(21)60020-3
27. Wang, Y., Qu, Q., Gao, S., Tang, G., Liu, K., He, S., Huang, C.: Biomass derived carbon as binder-free electrode materials for supercapacitors. Carbon N Y. 155, 706–726 (2019). https://doi.org/10.1016/j.carbon.2019.09.018
28. Kurian, M.: Recent progress in the chemical reduction of graphene oxide by green reductants–A Mini review. Carbon Trends. 5, 100120 (2021). https://doi.org/10.1016/j.cartre.2021.100120
29. Saini, S., Chand, P., Joshi, A.: Biomass derived carbon for supercapacitor applications: Review. J Energy Storage. 39, 102646 (2021). https://doi.org/10.1016/j.est.2021.102646
30. Lu, H., Zhao, X.S.: Biomass-derived carbon electrode materials for supercapacitors. Sustain Energy Fuels. 1, 1265–1281 (2017). https://doi.org/10.1039/C7SE00099E
31. Jyoti, K., Baunthiyal, M., Singh, A.: Characterization of silver nanoparticles synthesized using Urtica dioica Linn. leaves and their synergistic effects with antibiotics. J Radiat Res Appl Sci. 9, 217–227 (2016). https://doi.org/10.1016/j.jrras.2015.10.002
32. Majewska, J., Michalkiewicz, B.: Low temperature one-step synthesis of cobalt nanowires encapsulated in carbon. Applied Physics A. 111, 1013–1016 (2013).

https://doi.org/10.1007/s00339-013-7698-z

33. Benitha, V.S., Jeyasubramanian, K., Hikku, G.S.: Investigation of anti-corrosion ability of nano mixed metal oxide pigment dispersed alkyd coating and its optimization for A36 steel. J Alloys Compd. 721, 563–576 (2017). https://doi.org/10.1016/j.jallcom.2017.05.329
34. Sharma, H.K., Archana, R., Sankar ganesh, R., Singh, B.P., Ponnusamy, S., Hayakawa, Y., Muthamizhchelvan, C., Raji, P., Kim, D.Y., Sharma, S.K.: Substitution of Al3+ to Zn2+ sites of ZnO enhanced the photocatalytic degradation of methylene blue under irradiation of visible light. Solid State Sci. 94, 45–53 (2019). https://doi.org/10.1016/j.solidstatesciences.2019.05.011
35. Tavakoli, P., Shadizadeh, S.R., Hayati, F., Fattahi, M.: Effects of synthesized nanoparticles and Henna-Tragacanth solutions on oil/water interfacial tension: Nanofluids stability considerations. Petroleum. 6, 293–303 (2020). https://doi.org/10.1016/j.petlm.2020.03.001
36. Thirumalai, S., Shanmugavel, B.P.: Microwave Assisted Synthesis and Characterization of Barium Titanate Nanoparticles for Multi Layered Ceramic Capacitor Applications. Journal of Microwave Power and Electromagnetic Energy. 45, 121–127 (2011). https://doi.org/10.1080/08327823.2011.11689806
37. Singh, H., Du, J., Singh, P., Yi, T.H.: Ecofriendly synthesis of silver and gold nanoparticles by *Euphrasia officinalis* leaf extract and its biomedical applications. Artif Cells Nanomed Biotechnol. 46, 1163–1170 (2018). https://doi.org/10.1080/21691401.2017.1362417
38. Schneider, C., Walker, S., Phounglamcheik, A., Umeki, K., Kolb, T.: Effect of calcium dispersion and graphitization during high-temperature pyrolysis of beech wood char on the gasification rate with CO2. Fuel. 283, 118826 (2021). https://doi.org/10.1016/j.fuel.2020.118826
39. Uskoković, V.: A historical review of glassy carbon: Synthesis, structure, properties and applications. Carbon Trends. 5, 100116 (2021). https://doi.org/10.1016/j.cartre.2021.100116
40. Thangappan, R., Arivanandhan, M., Kalaiselvam, S., Jayavel, R., Hayakawa, Y.: Molybdenum Oxide/Graphene Nanocomposite Electrodes with Enhanced Capacitive Performance for Supercapacitor Applications. J Inorg Organomet Polym Mater. 28, 50–62 (2018). https://doi.org/10.1007/s10904-017-0699-1
41. Wang, C., Song, Z., Shi, P., Lv, L., Wan, H., Tao, L., Zhang, J., Wang, H., Wang, H.: High-rate transition metal-based cathode materials for battery-supercapacitor hybrid devices. Nanoscale Adv. 3, 5222–5239 (2021). https://doi.org/10.1039/D1NA00523E
42. Ghebache, Z., Safidine, Z., Hamidouche, F., Boudieb, N., Benaboura, A., Trari, M.: Effect of Hematite on the Energy Storage Performance of Polyaniline/Zeolite HY/α-Fe2O3 Nanocomposite Supercapacitor Electrode. J Inorg Organomet Polym Mater. 31, 1153–1162 (2021). https://doi.org/10.1007/s10904-020-01801-5
43. Prabhin, V.S., Jeyasubramanian, K., Jeyaseeli Rashmi, I., Hikku, G.S., Veluswamy, P., Cho, B.J.: Investigation of electrochemical capacitance of 18k nanoporous current collector incorporated MnO2. Mater Chem Phys. 220, 128–136 (2018). https://doi.org/10.1016/j.matchemphys.2018.08.056

44. Jeyasubramanian, K., Prabhin, V.S., Hikku, G.S., Preethi, A.V.M.: Investigation of super-capacitive nature of reduced graphene oxide nano mesh grown over 18 k gold foil using wings of Parides iphidamas as biological template. Mater Res Bull. 98, 25–33 (2018). https://doi.org/10.1016/j.materresbull.2017.09.051
45. Jing, C., Liu, X., Liu, X., Jiang, D., Dong, B., Dong, F., Wang, J., Li, N., Lan, T., Zhang, Y.: Crystal morphology evolution of Ni–Co layered double hydroxide nanostructure towards high-performance biotemplate asymmetric supercapacitors. CrystEngComm. 20, 7428–7434 (2018). https://doi.org/10.1039/C8CE01607K
46. Zhang, Q., Liu, X., Fan, W., Wang, Y.: Manganese-promoted cobalt oxide as efficient and stable non-noble metal catalyst for preferential oxidation of CO in H2 stream. Appl Catal B. 102, 207–214 (2011). https://doi.org/10.1016/j.apcatb.2010.11.043
47. Yang, W., Wang, P., Tu, Z., Hou, L., Yan, L., Jiang, B., Zhang, C., Huang, G., Yang, F., Li, Y.: Heteroatoms-doped hierarchical porous carbon with multi-scale structure derived from petroleum asphalt for high-performance supercapacitors. Carbon N Y. 187, 338–348 (2022). https://doi.org/10.1016/j.carbon.2021.11.008
48. Shao, S., Zhang, L., Liu, W., Zhang, Y., Shen, X., Nie, Y., Yang, W., Liu, H., Li, S., Li, S.: Synthesis of Hierarchical Porous MOFs via Ligand Thermolysis for High-Performance Supercapacitor. J Inorg Organomet Polym Mater. 32, 4412–4421 (2022). https://doi.org/10.1007/s10904-022-02427-5
49. Li, Y., Liang, Y., Liang, Y., Liu, Y., Xiao, Y.: Capillary enhanced hydrophilic block carbon material for binder-free supercapacitor electrode. J Power Sources. 507, 230289 (2021). https://doi.org/10.1016/j.jpowsour.2021.230289
50. Wu, X., Liu, R., Zhao, J., Fan, Z.: Advanced carbon materials with different spatial dimensions for supercapacitors. Nano Materials Science. 3, 241–267 (2021). https://doi.org/10.1016/j.nanoms.2021.01.002
51. Wu, S., Zhang, J., Sun, C., Chen, J.: Synthesis of MnO2/NiCo-Layered Double Hydroxide Hybrid as Electrode Materials for Supercapacitor. J Inorg Organomet Polym Mater. 30, 3179–3187 (2020). https://doi.org/10.1007/s10904-020-01481-1
52. Ghebache, Z., Hamidouche, F., Safidine, Z., Trari, M., Bellal, B.: Synthesis and Electrical Conducting Properties of Poly(aniline) Doped With Zeolite HY Nanocomposites Containing SnO2 for High-Performance Supercapacitor Electrode. J Inorg Organomet Polym Mater. 29, 1548–1558 (2019). https://doi.org/10.1007/s10904-019-01118-y
53. Xu, W., Liu, L., Weng, W.: High-performance supercapacitor based on MnO/carbon nanofiber composite in extended potential windows. Electrochim Acta. 370, 137713 (2021). https://doi.org/10.1016/j.electacta.2021.137713
54. Kumar, S.: Activated carbon derived from natural sources and electrochemical capacitance of double layer capacitor.
55. Yao, Z., Yu, C., Dai, H., Zhou, J., Liu, X., Sun, G.: Hybrid fibers assembled from MoSe2/graphene heterostructures endow improved supercapacitive performance. Carbon N Y. 187, 165–172 (2022).

https://doi.org/10.1016/j.carbon.2021.11.009

56. Shen, H., Liu, E., Xiang, X., Huang, Z., Tian, Y., Wu, Y., Wu, Z., Xie, H.: A novel activated carbon for supercapacitors. Mater Res Bull. 47, 662–666 (2012). https://doi.org/10.1016/j.materresbull.2011.12.028
57. Farzana, R., Rajarao, R., Bhat, B.R., Sahajwalla, V.: Performance of an activated carbon supercapacitor electrode synthesised from waste Compact Discs (CDs). Journal of Industrial and Engineering Chemistry. 65, 387–396 (2018). https://doi.org/10.1016/j.jiec.2018.05.011
58. Liu, L., Zhao, H., Wang, Y., Fang, Y., Xie, J., Lei, Y.: Evaluating the Role of Nanostructured Current Collectors in Energy Storage Capability of Supercapacitor Electrodes with Thick Electroactive Materials Layers. Adv Funct Mater. 28, 1705107 (2018). https://doi.org/10.1002/adfm.201705107
59. Liu, C., Neale, Z.G., Cao, G.: Understanding electrochemical potentials of cathode materials in rechargeable batteries. Materials Today. 19, 109–123 (2016). https://doi.org/10.1016/j.mattod.2015.10.009
60. Silambarasan, M., Ramesh, P.S., Geetha, D., Ravikumar, K., Ali, H.E., Algarni, H., Soundhirarajan, P., Chandekar, K. v., Shkir, Mohd.: A Facile Preparation of Zinc Cobaltite (ZnCo2O4) Nanostructures for Promising Supercapacitor Applications. J Inorg Organomet Polym Mater. 31, 3905–3920 (2021). https://doi.org/10.1007/s10904-021-02077-z
61. Afsharpour, M., Bayatpour, S., Seifikar Gomi, L.: Inorganic–Organic Hybrids of Tungsten Oxide as the High Performance Intercalation Supercapacitor Electrodes. J Inorg Organomet Polym Mater. 30, 2406–2417 (2020). https://doi.org/10.1007/s10904-019-01422-7
62. Prabhin, V.S., Jeyasubramanian, K., Benitha, V.S., Veluswamy, P., Cho, B.J.: Fabrication and evaluation of hybrid supercapacitor consisting of nano cobalt oxide and manganese oxide deposited electrochemically on nanoporous Au-Electrode. Electrochim Acta. 330, 135199 (2020). https://doi.org/10.1016/j.electacta.2019.135199
63. Inamdar, A.I., Kim, Y.S., Sohn, J.S., Im, H., Kim, H., Kim, D.-Y., Kalubarme, R.S., Park, C.: Supercapacitive Characteristics of Electrodeposited Polyaniline Thin Films Grown on Indium-doped Tin-oxide Substrates. Journal of the Korean Physical Society. 59, 145–149 (2011). https://doi.org/10.3938/jkps.59.145
64. Salunkhe, A.D., Pagare, P.K., Torane, A.P.: Review on Recent Modifications in Nickel Metal-Organic Framework Derived Electrode (Ni-MOF) Materials for Supercapacitors. J Inorg Organomet Polym Mater. (2022). https://doi.org/10.1007/s10904-022-02503-w
65. Nathan, D.M.G.T., Boby, S.J.M.: Hydrothermal preparation of hematite nanotubes/reduced graphene oxide nanocomposites as electrode material for high performance supercapacitors. J Alloys Compd. 700, 67–74 (2017). https://doi.org/10.1016/j.jallcom.2017.01.070
66. Yao, B., Peng, H., Zhang, H., Kang, J., Zhu, C., Delgado, G., Byrne, D., Faulkner, S., Freyman, M., Lu, X., Worsley, M.A., Lu, J.Q., Li, Y.: Printing Porous Carbon Aerogels for Low Temperature Supercapacitors. Nano Lett. 21, 3731–3737 (2021). https://doi.org/10.1021/acs.nanolett.0c04780

67. Wu, Y., Cao, J.-P., Zhuang, Q.-Q., Zhao, X.-Y., Zhou, Z., Wei, Y.-L., Zhao, M., Bai, H.-C.: Biomass-derived three-dimensional hierarchical porous carbon network for symmetric supercapacitors with ultra-high energy density in ionic liquid electrolyte. Electrochim Acta. 371, 137825 (2021). https://doi.org/10.1016/j.electacta.2021.137825
68. Jayachandiran, J., Yesuraj, J., Arivanandhan, M., Raja, A., Suthanthiraraj, S.A., Jayavel, R., Nedumaran, D.: Synthesis and Electrochemical Studies of rGO/ZnO Nanocomposite for Supercapacitor Application. J Inorg Organomet Polym Mater. 28, 2046–2055 (2018). https://doi.org/10.1007/s10904-018-0873-0
69. Yang, W., Wang, P., Tu, Z., Hou, L., Yan, L., Jiang, B., Zhang, C., Huang, G., Yang, F., Li, Y.: Heteroatoms-doped hierarchical porous carbon with multi-scale structure derived from petroleum asphalt for high-performance supercapacitors. Carbon N Y. 187, 338–348 (2022). https://doi.org/10.1016/j.carbon.2021.11.008
70. Kurtan, U., Sahinturk, U., Aydın, H., Dursun, D., Baykal, A.: CoFe Nanoparticles in Carbon Nanofibers as an Electrode for Ultra-Stable Supercapacitor. J Inorg Organomet Polym Mater. 30, 3608–3616 (2020). https://doi.org/10.1007/s10904-020-01524-7
71. Kung, C.-Y., Wang, T.-L., Lin, H.-Y., Yang, C.-H.: A high-performance covalently bonded self-doped polyaniline–graphene assembly film with superior stability for supercapacitors. J Power Sources. 490, 229538 (2021). https://doi.org/10.1016/j.jpowsour.2021.229538
72. Mariappan, V.K., Krishnamoorthy, K., Pazhamalai, P., Sahoo, S., Kim, S.-J.: Layered famatinite nanoplates as an advanced pseudocapacitive electrode material for supercapacitor applications. Electrochim Acta. 275, 110–118 (2018). https://doi.org/10.1016/j.electacta.2018.04.126
73. Krishnamoorthy, K., Pazhamalai, P., Sahoo, S., Kim, S.-J.: Titanium carbide sheet based high performance wire type solid state supercapacitors. J Mater Chem A Mater. 5, 5726–5736 (2017). https://doi.org/10.1039/C6TA11198J
74. Howli, P., Das, S., Sarkar, S., Samanta, M., Panigrahi, K., Das, N.S., Chattopadhyay, K.K.: Co_3O_4 Nanowires on Flexible Carbon Fabric as a Binder-Free Electrode for All Solid-State Symmetric Supercapacitor. ACS Omega. 2, 4216–4226 (2017). https://doi.org/10.1021/acsomega.7b00702
75. Iurilli, P., Brivio, C., Wood, V.: On the use of electrochemical impedance spectroscopy to characterize and model the aging phenomena of lithium-ion batteries: a critical review. J Power Sources. 505, 229860 (2021). https://doi.org/10.1016/j.jpowsour.2021.229860
76. Wang, X., Wei, X., Dai, H.: Estimation of state of health of lithium-ion batteries based on charge transfer resistance considering different temperature and state of charge. J Energy Storage. 21, 618–631 (2019). https://doi.org/10.1016/j.est.2018.11.020
77. Zhao, C., Lin, L., Tian, S., Nie, P., Xue, X., Wang, H., Xu, T., Chang, L.: Facile Fabrication of Binder-Free CoZn LDH/CFP Electrode with Enhanced Capacitive Properties for Asymmetric Supercapacitor. J Inorg Organomet Polym Mater. 31, 3953–3961 (2021). https://doi.org/10.1007/s10904-021-02023-z
78. M., A., Paul, A.: Importance of Electrode Preparation Methodologies in Supercapacitor Applications. ACS Omega. 2, 8039–8050 (2017). https://doi.org/10.1021/acsomega.7b01275

Scheme

Scheme 1 is available in the Supplementary Files section.

Figures

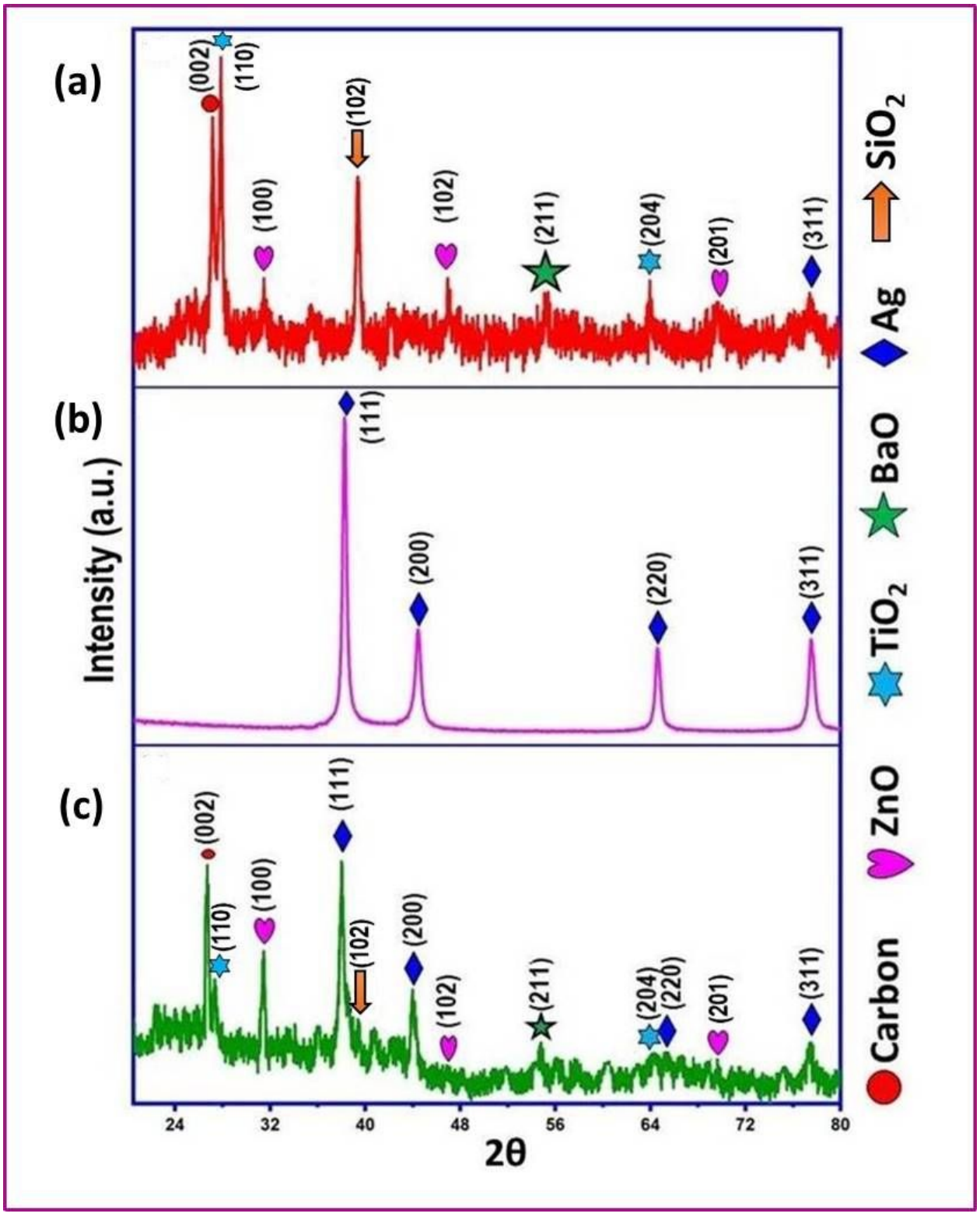

Figure 1

XRD pattern of (a) DESTP (b) Ag and (c) Ag@DESTP

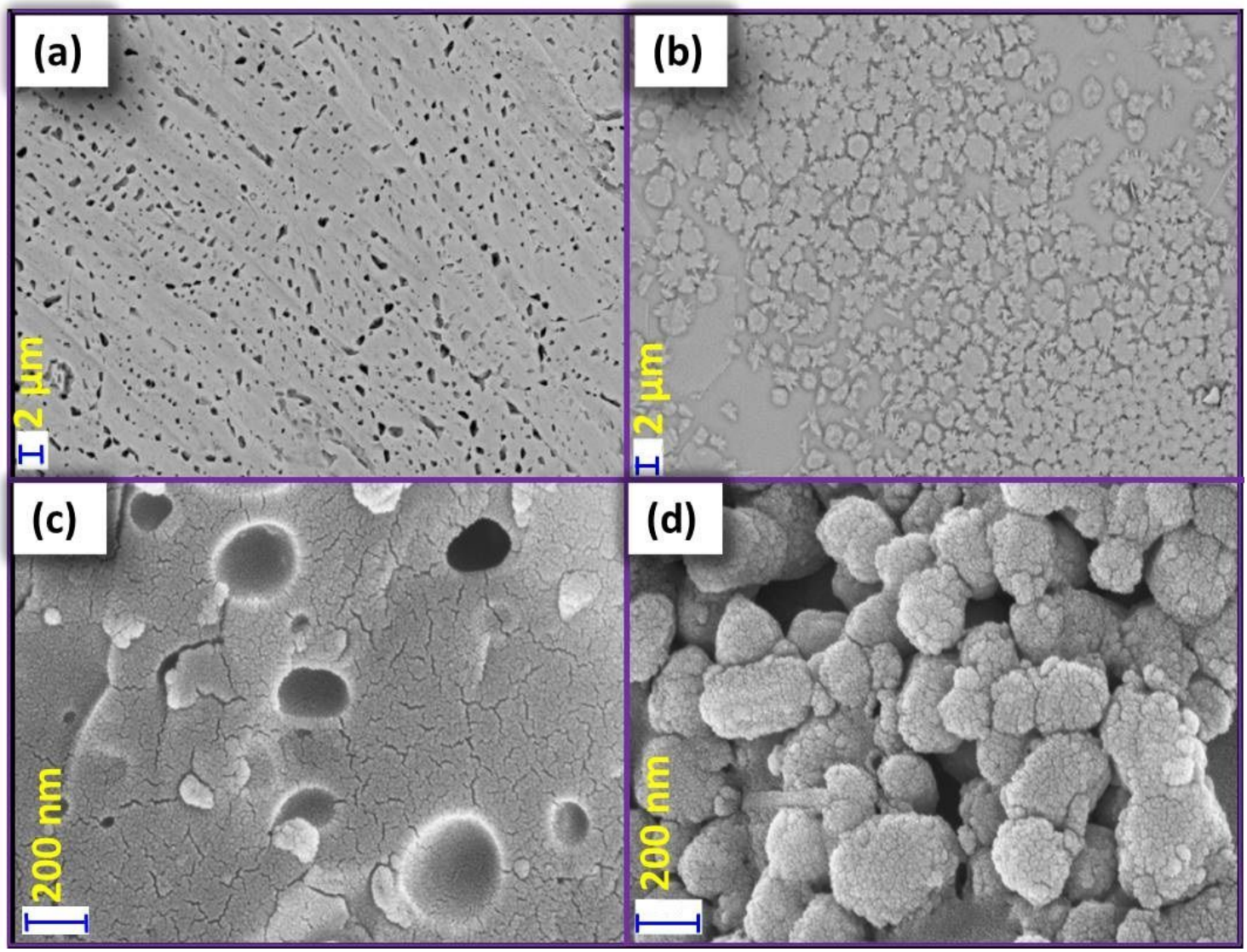

Figure 2

FESEM images (a) Brass (b) Etched Brass (c) DESTP and (d) Ag@DESTP

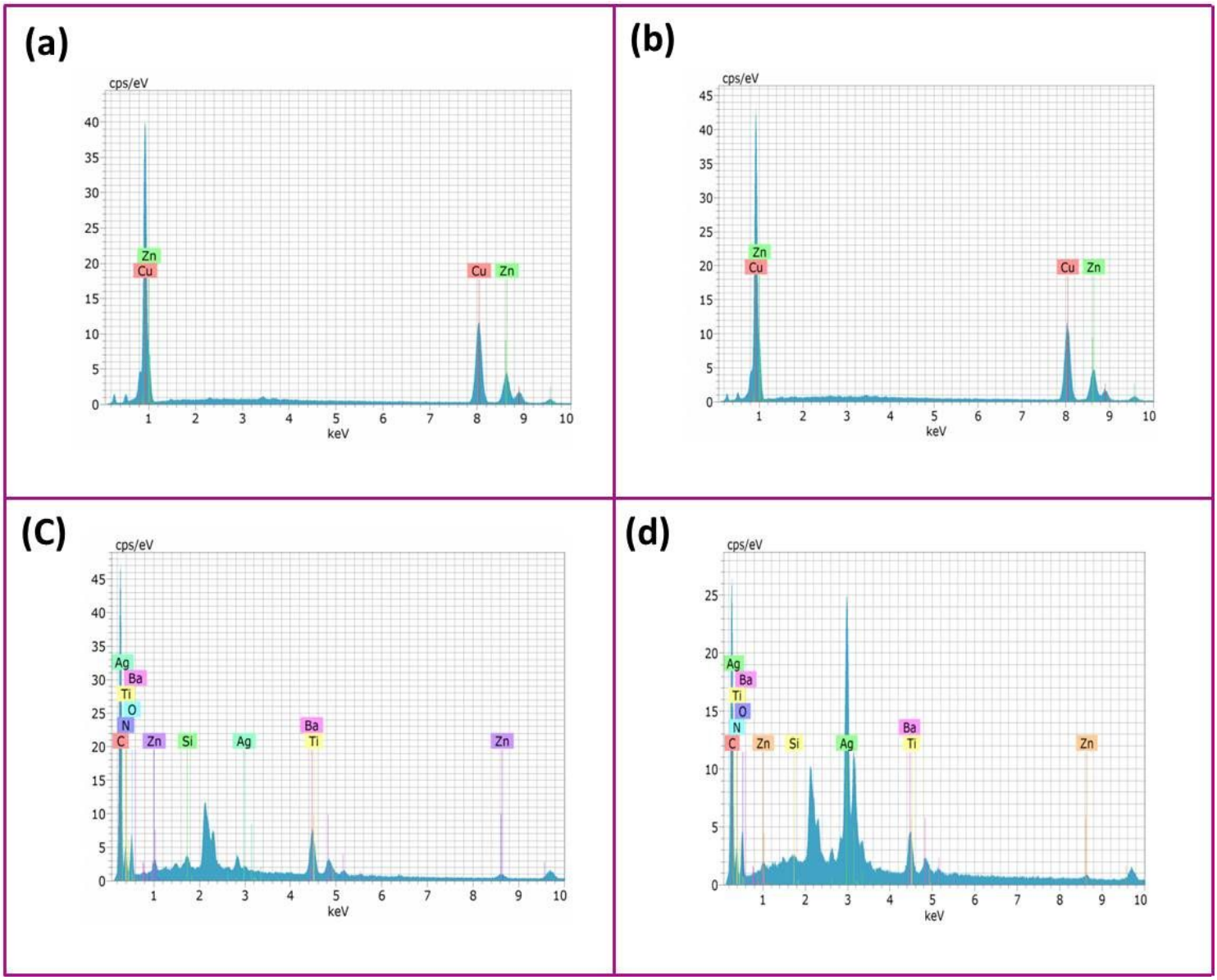

Figure 3

EDAX spectra (a) Brass (b) Etched Brass (c) DESTP and (d) Ag@DESTP

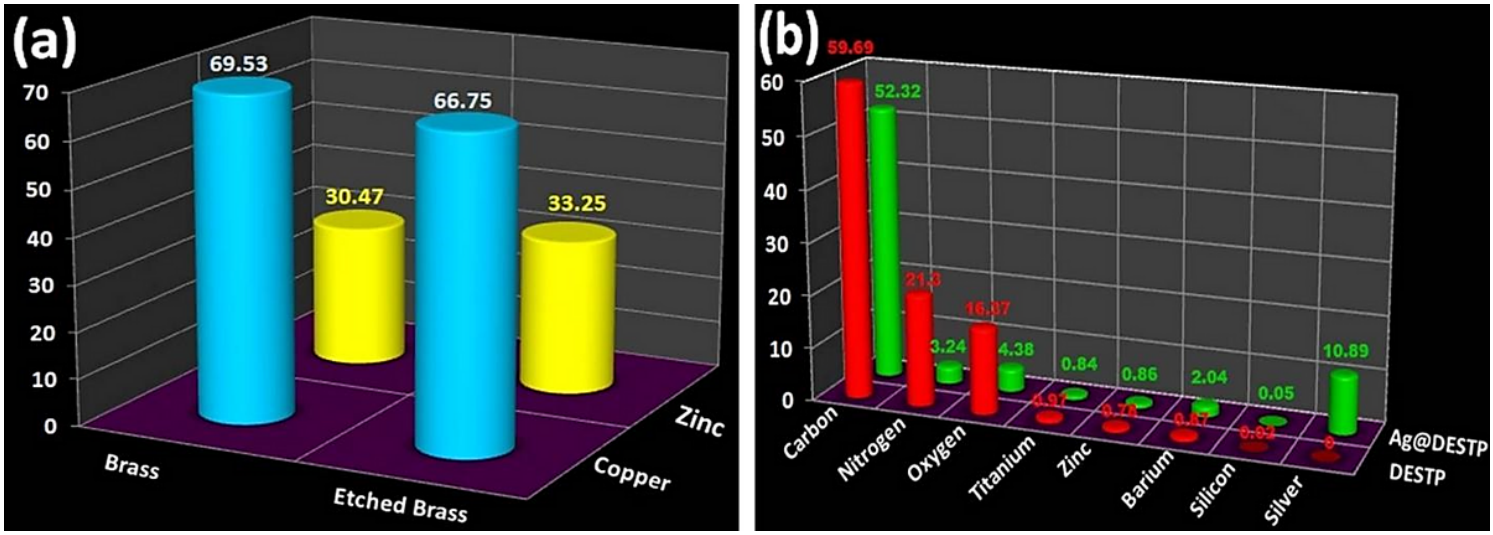

Figure 4

Elemental composition of (a) brass and etched brass (b) DESTP and Ag@DESTP

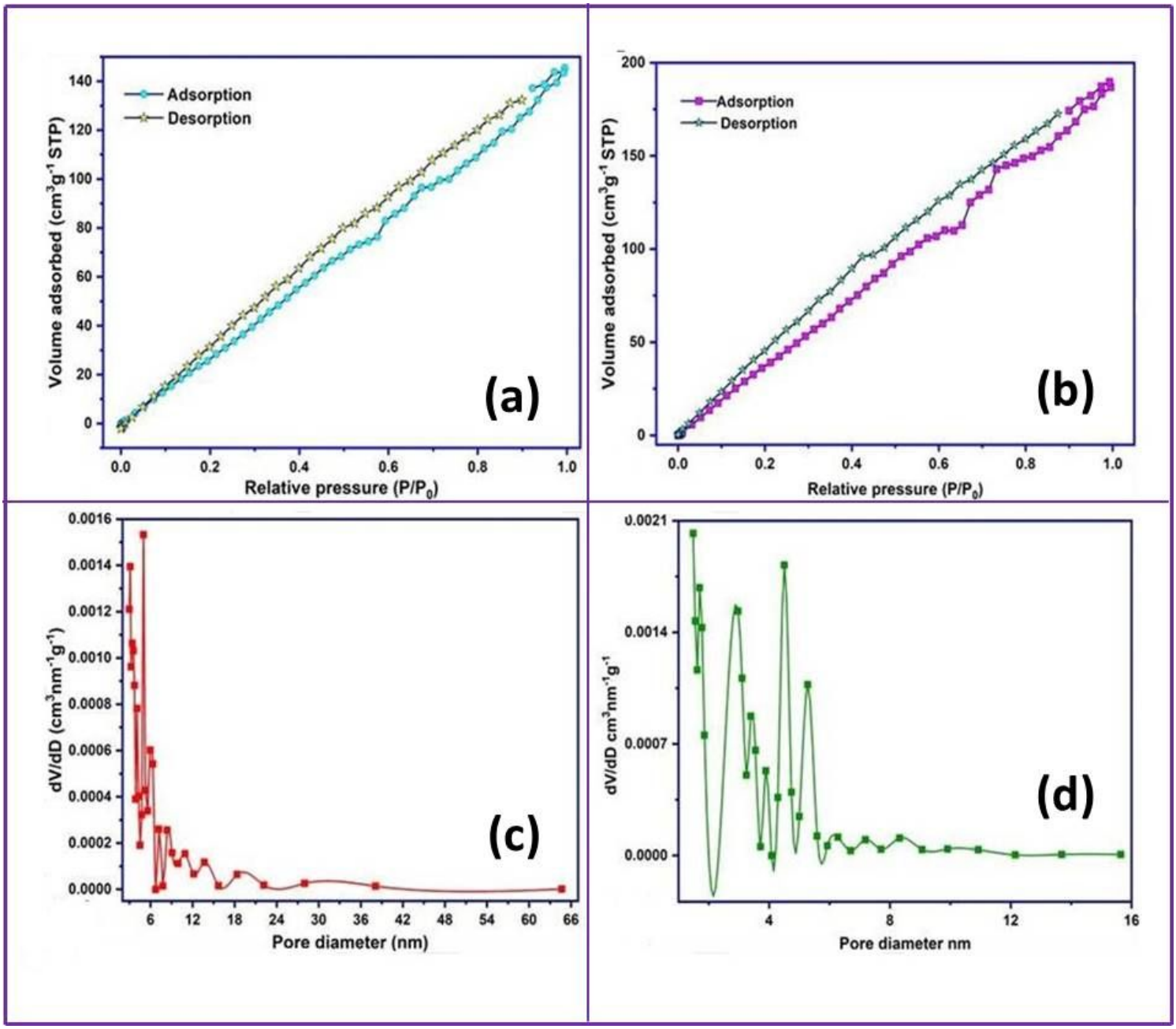

Figure 5

(a & b) N_2 absorption/desorption isotherms of DESTP and Ag@DESTP and (c & d) BJH pore size scattering plot of DESTP and Ag@DESTP.

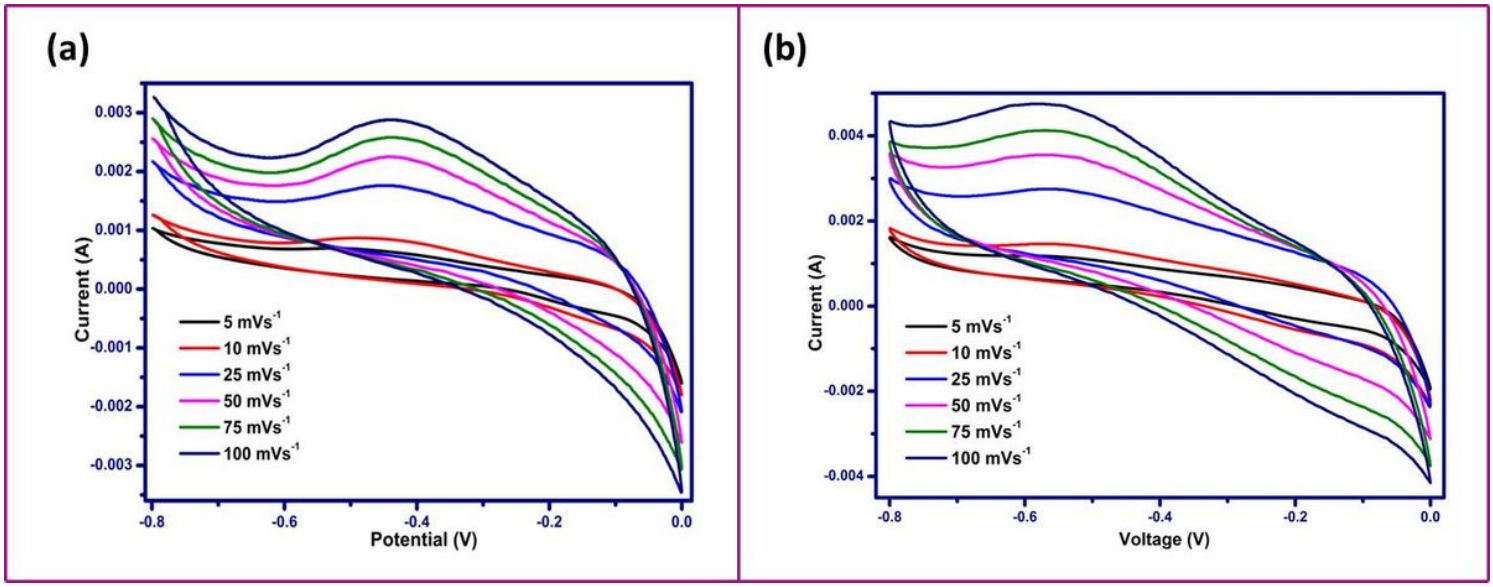

Figure 6

CV graphs recorded at different scan rates between 5 mVs^{-1} and 100 mVs^{-1} (a) DESTP and (b) Ag-DESTP.

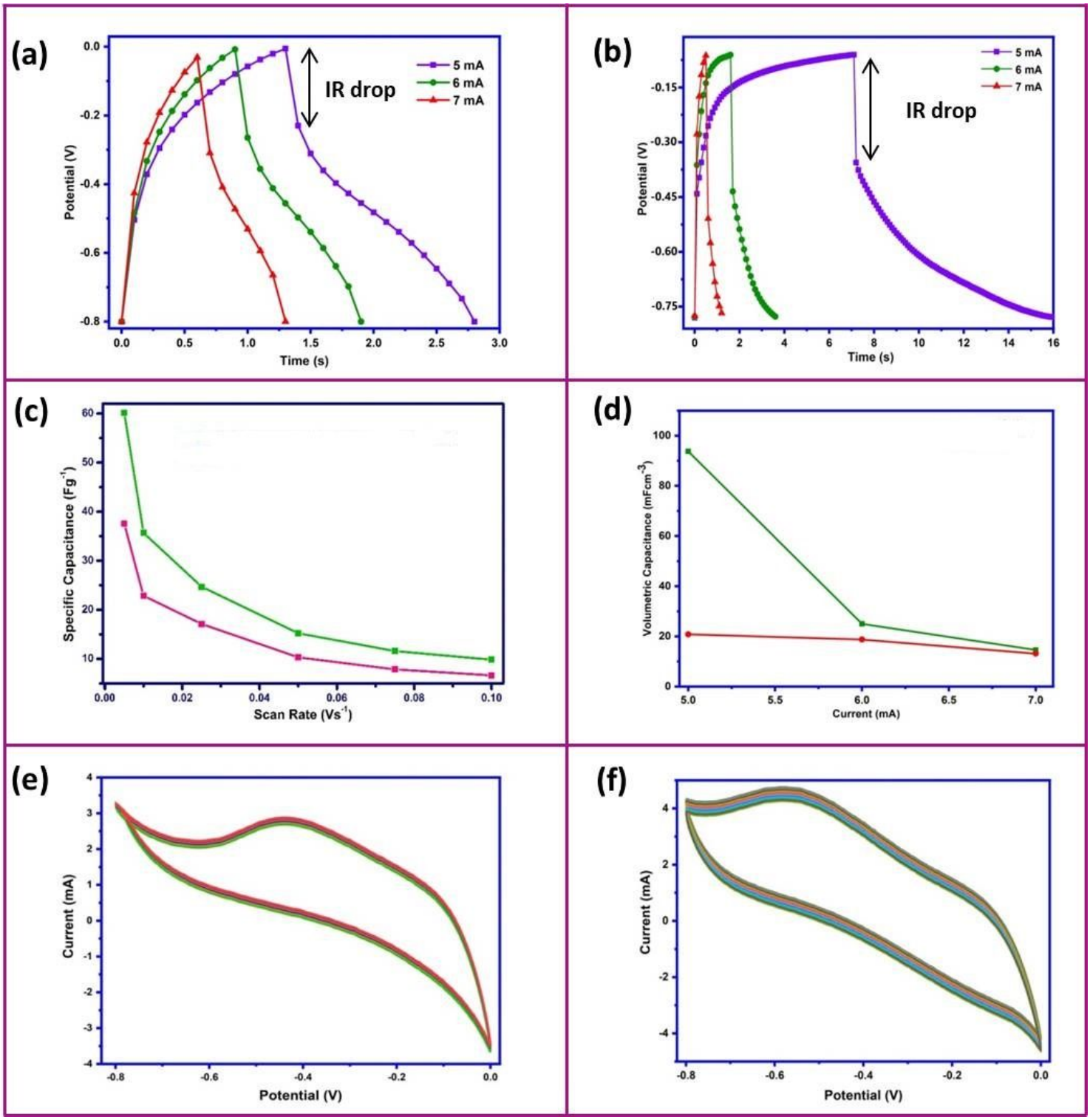

Figure 7

(a) & (b)Galvanostatic charge discharge voltage profiles between 5mA to 7 mA of DESTP and Ag@DESTP electrodes, (c) & (d) Specific capacitance with respect to different scan rates between 5 mVs^{-1} and 100 $mVs^{-1}$and current density, (e) & (f) specific capacitance retention curves for DESTP and Ag@DESTP electrode for 5000 cycles at the scan rate of 100 mVs^{-1}

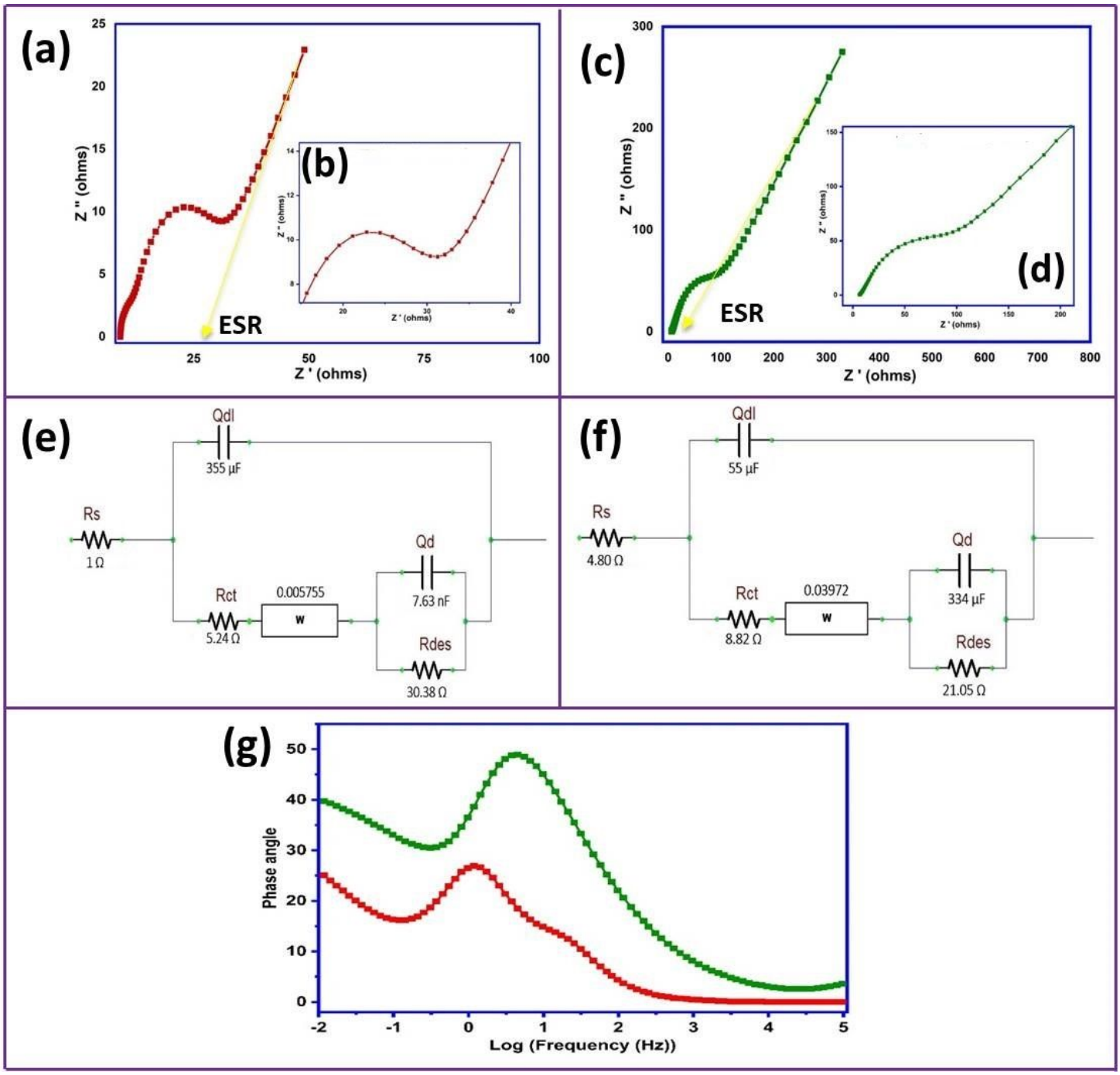

Figure 8

EIS studies(a) & (c)Nyquist plot of DESTP and Ag@DESTP, (b) & (d) Zoomed image of(a) & (c), (e) & (f) Equivalent circuit of Ag@DESTP and DESTP, (g) Phase angle plot of DESTP and Ag@DESTP electrodes.

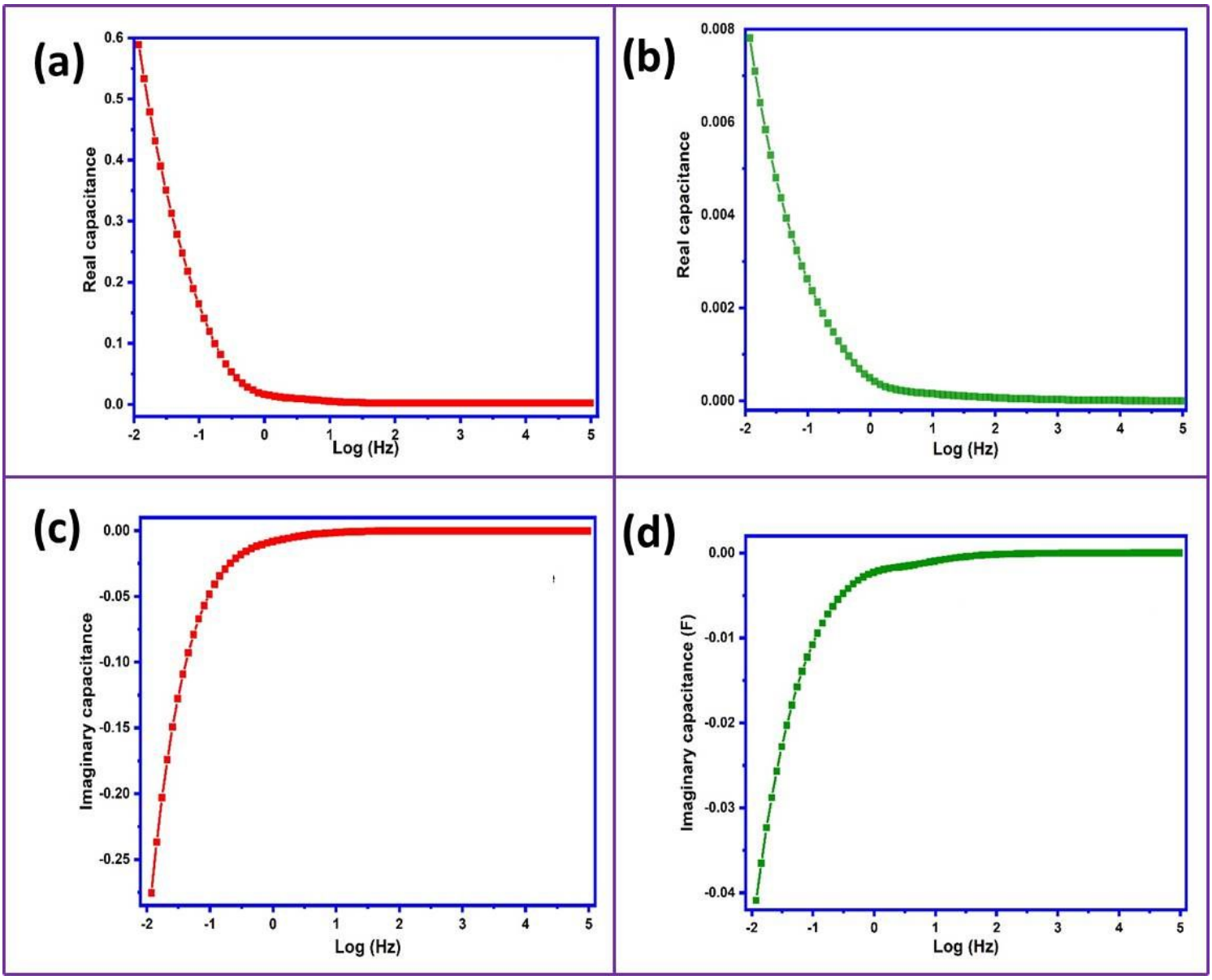

Figure 9

(a) & (b) Real capacitance of DESTP and Ag@DESTP electrode, (c) & (d) Imaginary capacitance of DESTP and Ag@DESTP electrode.

Supplementary Files

This is a list of supplementary files associated with this preprint. Click to download.

- floatimage1.jpeg